Leukocyte differentiation by histidine-rich glycoprotein/stanniocalcin-2 complex regulates murine glioma growth through modulation of anti-tumor immunity

Francis P. Roche[1)], Ilkka Pietilä[2)*], Hiroshi Kaito[1)*], Elisabet O. Sjöström[1)], Nadine Sobotzki[3)], Oriol Noguer[1)], Tor Persson Skare[1)], Magnus Essand[1)], Bernd Wollscheid[3)], Michael Welsh[2)] and Lena Claesson-Welsh[1,∞)]

1) Uppsala University, Department of Immunology, Genetics and Pathology, Science for Life Laboratory, The Rudbeck Laboratory, Dag Hammarskjöldsv. 20, 751 85 Uppsala, Sweden.

2) Uppsala University, Department of Medical Cell Biology, Biomedical Center, Box 571, 751 23 Uppsala, Sweden

3) ETH Zürich, Department of Health Sciences and Technology & Institute of Molecular Systems Biology, Auguste-Picard-Hof 1, 8093 Zürich, Switzerland

*indicates equal contribution

∞) Correspondence to Lena Claesson-Welsh at the address above, email lena.welsh@igp.uu.se, or phone +46-70 167 9260

Author email addresses: Francis P. Roche (rochefp@tcd.ie), Pietilä (ilkka.pietila@mcb.uu.se), Hiroshi Kaito (hkaitoh@gmail.com), Elisabet O. Sjöstrom (ohlinelisabet@gmail.com), Nadine Sobotzki (sobotzki@imsb.biol.ethz.ch), Oriol Noguer (oriolnoguerserra@gmail.com), Tor Persson Skare (tor.persson@igp.uu.se), Magnus Essand (magnus.essand@igp.uu.se), Bernd Wollscheid (bernd.wollscheid@hest.ethz.ch), Michael Welsh (Michael.welsh@mcb.uu.se), Lena Claesson-Welsh (lena.welsh@igp.uu.se)

Key words: HRG, STC2, glioma, anti-tumor immunity, immunomodulation, CD45, CD8, Treg

Running title: Glioma inflammation regulated by HRG

Category: **Large Molecule Therapeutics**

Text word count: 4,936
Abstract word count: 212
Number of figures and tables: 6 figures, 2 tables
Number of references: 48

Abbreviations

Ad5; adenovirus type 5, BSA; bovine serum albumin, CNS; central nervous system, CSF-1; colony stimulating factor-1, CTLA4; cytotoxic T-lymphocyte-associated protein 4, DAPI; 4,6 diamidino-2-phenylindole, DMSO; Dimethyl sulfoxide, dpi; days post infection, Ebi3; Epstein-Barr virus induced gene 3, ELISA; enzyme-linked immunosorbent assay, FACS; fluorescence activated cell sorting, ffu; focus forming units, GO; gene ontology, hpi; hours post infection, HRG; histidine-rich glycoprotein, IL; interleukin, IgG; immunoglobulin, MOI; multiplicity of infection, MRC1; C-type mannose receptor 1, MS; mass spectrometry, PBS; phosphate-buffered saline, PD1; programmed cell death 1, PD-L1; CD274, STC2; stanniocalcin-2, TMZ; temozolomide, VitD3; vitamin D_3/25 α-dihydroxicholecalciferol.

Conflict-of-interest disclosure: FPR, IP, HK, EOS, ON, TPS, ME, MW and LCW declare no conflict of interest. NS and BW give the following declaration: The TRICEPS and HATRIC compounds are patented (EP11000731 & EP15003213) with Nadine Sobotzki (EP15003213) and Bernd Wollscheid (EP11000731 & EP15003213) listed as inventors. The patents are licensed to Dualsystems Biotech AG (Schlieren, Switzerland) by ETH Zurich.

Financial disclosure: The authors declare no competing financial interests.

Abstract

The plasma-protein histidine-rich glycoprotein (HRG) is implicated in phenotypic switching of tumor-associated macrophages, regulating cytokine production and phagocytotic activity, thereby promoting vessel normalization and anti-tumor immune responses. To assess the therapeutic effect of HRG gene delivery on CNS tumors, we used adenovirus-encoded HRG to treat mouse intracranial GL261 glioma. Delivery of Ad5-HRG to the tumor site resulted in a significant reduction in glioma growth, associated with increased vessel perfusion and increased $CD45^+$ leukocyte and $CD8^+$ T cell accumulation in the tumor. Antibody-mediated neutralization of colony-stimulating factor-1 suppressed the effects of HRG on $CD45^+$ and $CD8^+$ infiltration. Using a novel protein interaction-decoding technology, TRICEPS-based ligand receptor capture (LRC), we identified Stanniocalcin-2 (STC2) as an interacting partner of HRG on the surface of inflammatory cells *in vitro* and co-localization of HRG and STC2 in gliomas. HRG reduced the suppressive effects of STC2 on monocyte $CD14^+$ differentiation and STC2-regulated immune response pathways. In consequence, Ad5-HRG treated gliomas displayed decreased numbers of Interleukin-35^+ Treg cells, providing a mechanistic rationale for the reduction in GL261 growth in response to Ad5-HRG delivery. We conclude that HRG suppresses glioma growth by modulating tumor inflammation through monocyte infiltration and differentiation. Moreover, HRG acts to balance the regulatory effects of its partner, STC2, on inflammation and innate and/or acquired immunity. HRG gene delivery therefore offers a potential therapeutic strategy to control anti-tumor immunity.

Introduction

Histidine-rich glycoprotein (HRG) is a cation- and heparin-binding, 75 kDa plasma glycoprotein produced by liver hepatocytes, present in blood at a concentration of 150 μg/ml (2 μM) (1). HRG comprises two N-terminal cystatin domains, and a C-terminal His/Pro-rich repeat region (2). The plasma levels of HRG in healthy adults are stable although the protein is continuously taken up and turned over by leukocytes (3). HRG binds heparan sulfate with high affinity (4). It also binds to several components of the complement system (5) and to immunoglobulins (6), thereby enhancing macrophage phagocytosis of necrotic material and immune complexes (5, 6) in a manner dependent on Zn^{2+}-binding to the His/Pro region (7). HRG has also been shown to possess antimicrobial activity (8).

HRG has been implicated in cancer growth and spread by influencing endothelial cell adhesion and migration, through interactions with integrin adhesion complexes (9, 10). Moreover, HRG affects cancer inflammation and immunity by direct gene regulatory effects on tumor-infiltrating leukocytes (11). In several mouse tumor models (4T1 breast cancer, Panc02 pancreatic cancer and T241 fibrosarcoma), HRG therapy promotes M1 polarization of tumor-associated macrophages (TAMs) *in vitro* and *in vivo* (12). The M1 polarization is accompanied by reduced production of pro-angiogenic and pro-tumoral stimulation, resulting in normalization of tumor vessel morphology and perfusion, reduced metastatic spread and enhanced chemotherapy delivery and efficacy. Additionally, HRG promotes anti-tumor immunity via increased dendritic cell (DC), natural killer (NK) and T cell tumor infiltration as a consequence of specific cytokine production by HRG-treated M1 macrophages (11). Conversely, the *Hrg* knockout mouse displays accelerated tumor growth and spread and marked upregulation of M2 markers such as interleukin (IL)-10, in peritoneal macrophages (13). The naïve *Hrg* knockout mouse presents with enhanced coagulation and fibrinolysis but otherwise lacks an overt phenotype (14).

We have previously shown that iodinated HRG becomes enriched on spleen leukocytes when administered to the circulation in mice and that cultured inflammatory cells specifically bind HRG (3). Using a recently developed protein interaction decoding technology, TRICEPS-based Ligand Receptor Capture (LRC) technology (15, 16), we presently identify Stanniocalcin-2 (STC2) as an HRG interacting partner, on the cell surface of inflammatory cells. STC2 is a heparin-binding, secreted homodimeric glycoprotein produced by several different cell types. Moreover, STC2 is implicated in negative regulation of tissue growth as *Stc2*-deficient mice show 10-15% increased weight and faster growth than wild type litter mates (17). STC2 expression correlates with malignancy and spread in different human cancer forms (18, 19). STC2 is upregulated in T cells developing a Th2 response (20) and it is a metagene, i.e. a gene with broad effects on biological processes that negatively correlate with immune-related metagenes in breast cancer transcript arrays (21).

Primary tumors of the central nervous system (CNS) represent a particularly complex target for therapeutic intervention highlighted by the lack of significant changes in 5-year survival rate in the last decades (22). The anatomical location severely restricts surgical intervention and, even when possible, the invasive growth pattern of gliomas rapidly results in tumor recurrence within the resection cuff. Despite the aggressive combination of radio- and chemotherapy, grade

4 gliomas remain almost invariably fatal. Recently, the anti-VEGF neutralizing antibody Bevacizumab has been added to the therapeutic regiment for glioblastoma and although 6-month progression free survival rates have increased, overall survival remains largely unchanged (23). There remains an urgent need for novel and/or neoadjuvant therapies.

Here we delivered HRG, using a non-replicating adenovirus-based vector, to orthotopically growing GL261 gliomas. The growth-suppressive effects of HRG on gliomas were paralleled by infiltration of STC2-expressing inflammatory cells. Moreover, HRG and STC2 individually and in complex regulated immune gene expression in inflammatory and immune cells. Thus, depending on the molecular configuration, HRG and STC2 may serve essential roles in steering inflammatory cell polarity to positively or negatively regulate immune and inflammatory pathways in cancer.

Methods

See online supplemental material for methodology not described below.

Animal studies

Subcutaneous Panc02 (24) tumor studies were carried out in 8-10 weeks male C57Bl/6 mice. Panc02 cells were cultured in DMEM GlutaMAX medium (Gibco), 10% FBS and used for injection on the back of mice ($2.5x10^5$ cells/mouse). When tumors reached 50 mm^3 in size, Ad-Empty, Ad-HRG or Ad-HRG-Luc vectors (25) ($5x10^8$ ffu), were injected intratumorally. Blood was sampled over 21 days by sub-mandibular vein bleeding (26) into ethylenediaminetetraacetic acid (EDTA)-coated tubes and snap-frozen. Additionally, mice were injected with D-luciferin intraperitoneally (100 mg/kg) and imaged on the IVIS live-imaging system.

To establish intracerebral glioma (27) in 8-10 weeks female C57Bl/6 mice, GL261 cells, cultured in DMEM GlutaMAX medium (Gibco), 10% FBS, were used for injection according to Lal and coworkers (28). Briefly, an implantable guide screw was placed in the skull at coordinates dorsal to the caudate nucleus (+1 mm anteroposterior, -2.3 medial-lateral from bregma**).** One week later (day 1), GL261 cell inoculation was carried out by injecting 7,500 cells in 0.5 ul, at a depth of 4.5 mm from the top of the screw (corresponding to -2.5 mm from the dorsal cortical surface). Six days later (day 7), a small incision above the guide screw was made and adenovirus vectors ($7x10^7$ ffu) were injected at coordinates corresponding to the inoculation site, followed, 6 days later (day 13), by a second injection. Twentyone days after GL261 cell inoculation, animals were given an intravenous injection of biotinylated-tomato lectin (4 mg/kg, Vector Labs), and circulated for 10 minutes followed by terminal anesthesia with xylazine/ketamine and transcardiac perfusion with PBS and 4% paraformaldehyde/PBS. Brains were dissected, post-fixed in paraformaldehyde for 4 hours at 4°C, and incubated overnight in 30% sucrose, 4°C. Prepared brains were vibratome-sectioned into 100 μm coronal sections, mounted onto superfrost glass and distributed in 6 series covering the entire tumor. For tumor size estimation, one series was stained with H&E, images acquired on a Nikon Eclipse 80i and the tumor area/section determined by manual identification and automated quantification using the ImageJ analysis software. Final tumor area for each animal was determined by the sum of tumor area from each section in a single series.

For chemotherapy treatment, temozolomide (TMZ) was given by oral gavage in PBS/0.6% dimethylsulfoxide (DMSO). A dose-response curve was established by treating tumor-bearing mice with TMZ at a concentration range of 1.12 - 28 mg/kg/week. For co-treatment with Ad5, mice were given a TMZ dose corresponding to the IC20 (1 mg/kg/treatment corresponding to 3 mg/kg/week) from days 10-12 and 16-18.

For colony stimulating factor-1 (CSF1)-neutralizing antibody treatment, mice were treated by intraperitoneal injection with 1 mg antibody per mouse, either anti-CSF1 (Clone 5A1, BioXCell) or isotype control (BE0088, BioXCell).

Ethical and biosafety declaration

In vivo animal experiments were carried out in strict accordance with the ethical permit provided by the Committee on the Ethics of Animal Experiments of the University of Uppsala (Permit Numbers: C192/12, and C232/12). The Swedish Work Environment Authority has approved the

work with replication-defective adenoviral vectors encoding immunomodulatory transgenes (ID number 202100-2932 v66a16 and v76a5). All experiments regarding adenoviral-vectors were conducted under Biosafety level 2.

Cell line

The human monoblastic U937 cell line that differentiates towards monocyte/macrophage lineage in response to vitamin D_3 (29) was a kind gift from Prof. Helena Jernberg Wiklund, Uppsala University. Cells were tested negative for mycoplasma but was otherwise not authenticated.

Statistical analyses

Statistical analyses were done using one-way ANOVA followed by different tests (Fisher's LSD, Tukey's and Bonferroni's) depending on sample properties for comparison between multiple groups. Students' t-test or chi-square test was used for comparison between two groups. All experiments were repeated at least three times in an independent manner.

Results

Adenovirus production and expression analysis

Replication-deficient Ad5 vectors 1) lacking a transgene element (Ad5-Empty), 2) encoding murine HRG (Ad5-HRG), or 3) encoding HRG and Luciferase separated by a T2A auto-protease linker (Ad5-HRG-Luc), were tested for their properties by infection of pancreatic adenocarcinoma-derived Panc02 cells. HRG expression was evident from 24 hours post infection (hpi) in Ad5-HRG-Luc and Ad5-HRG-infected cell culture medium while absent from the Ad5-Empty infected control. HRG expression peaked at 48 hpi in Panc02 cells, corresponding to 600 ng HRG / $5x10^4$ cells (Figure S1A). Luciferase expression was present in Ad5-HRG-Luc infected cells only (Figure S1B). Expressed HRG protein harvested from the culture medium bound to heparin and inhibited the directed migration of endothelial cells, as expected (Figure S1C and S1D, respectively). Thus, HRG was robustly expressed from cells infected with Ad5-HRG-Luc or Ad5-HRG and, importantly, retained properties typical for HRG.

To examine the expression of Ad5 transgenes *in vivo*, subcutaneous Panc02 tumors were injected intratumorally with a single dose of $1x10^8$ ffu Ad5-Empty or Ad5-HRG-Luc. Luciferase activity was assayed by *in vivo* live luminescence imaging and systemic blood HRG levels assayed by ELISA. Luciferase expression peaked at 2 days post infection (dpi) and dropped off exponentially thereafter, but was evident until the experimental end point at 21 dpi (Figure 1A). Consistent with the known circulating levels of HRG in murine plasma, HRG was present at 150 µg/ml in peripheral blood prior to virus treatment. The HRG concentration in Ad5-HRG lysates from perfused Panc02 tumors showed a 3- to 6-fold increase compared to controls, PBS or Ad5-empty Panc02 tumors (Figure 1B). Tumor HRG expression in Ad5-HRG but not Ad5-Empty injected mice was verified by immunoblotting (Figure S2).

To examine the potential for the HRG adenovirus to suppress the growth of established tumors, subcutaneous Panc02 tumors were injected with buffer or $1x10^8$ ffu Ad5-Empty or Ad5-HRG. Injections started on firmly established tumors (50 mm^3) and were carried out every 4 days for a total of 4 injections. As shown in Figures 1C and D, treatment with Ad5-HRG significantly reduced established Panc02 tumor growth and mean tumor volume at the experimental endpoint.

HRG gene therapy of orthotopic GL261 glioma

To assess the potential therapeutic consequence of the Ad5-HRG treatment on orthotopic glioma we employed the guide screw system (28), which allows for repeated delivery of therapeutics to brain tumors. 7,500 GL261 glioma cells were injected via the guide cannula at coordinates corresponding to the caudate nucleus. GL261 is known to replicate phenotypic characteristics of the human glioblastoma such as invasive growth (27). Six days after implantation, buffer or virus (Ad5-empty or Ad5-HRG) was administered to the coordinates used for GL261 cell inoculation. A second treatment was delivered 6 days after the first injection and the animals were sacrificed on day 22 (Figure 2A). Ad5-HRG treatment demonstrated a significant inhibition of GL261 growth compared to Ad5-Empty and buffer-treated animals (Figure 2B). This pattern was seen robustly over three independent experiments using two independently produced and titered Ad5 batches.

HRG has previously demonstrated anti-tumor effects in different mouse tumor models, correlating with changes in vascular and immune cells parameters (11). Consistent with previous observations, Ad5-HRG treatment resulted in a significant increase in the total number and area of lectin-positive and therefore perfused vessels, compared to both Ad5-Empty and buffer treated animals (Figure 2C). The known role of $CD45^+$ positive cells in HRGs anti-tumor activity prompted the examination of changes in leukocyte numbers in treated tumors. Indeed, $CD45^+$ cells were specifically increased upon Ad5-HRG treatment (Figure 2D).

Ad5-HRG mechanism of action requires the presence of $CD45^+$ cells

CSF-1 neutralization is an effective strategy for reducing macrophage recruitment though the downregulation of macrophage cell survival, proliferation and differentiation (30). To determine the contribution of CSF1 receptor (CSF1R) expressing macrophages/monocytes to $CD45^+$ cells for the anti-tumor effect of HRG on glioma, we treated glioma-bearing animals with a neutralizing CSF1 antibody (Clone 5A1) in combination with intracerebral Ad5 vector injection. The αCSF1 Ab was delivered at a dose previously demonstrated to cause the specific loss of $CSFR1^+$ cells and macrophages (3), one day after glioma cell inoculation and at days 6, 10 and 14 (Figure 3A). Treatment with Ad5-HRG combined with control immunoglobulin (IgG) resulted in a 50% reduction in tumor size compared to the corresponding Ad5-Empty treated animals (Figure 3B). Importantly, treatment with Ad5-HRG/αCSF1 Ab did not further reduce glioma growth compared to Ad5-Empty/αCSF1 Ab or Ad5-Empty/control IgG (Figure 3B) (31). Moreover, treatment with the αCSF1 Ab, efficiently suppressed infiltration of CD45+ cells by Ad5-HRG (Figure 3C). That HRG failed to further suppress glioma growth when combined with the CSF1-neutralizing antibody is consistent with an essential role for CD45+/CSF1R+ macrophages in the mechanism of action of HRG. In addition, $CD8a^+$ T cells were reduced in Ad5-HRG/αCFS1 Ab treated tumors (Figure 3D). Although the changes in $CD8a^+$ cell infiltration did not reach significant differences, the trends followed the same pattern as the effects of HRG on $CD45^+$ cell infiltration, suggesting a possible relationship between these.

Temozolomide treatment antagonizes the effect of Ad5-HRG on tumor growth

To assess the potential for co-treatment of HRG with chemotherapy, the DNA alkylating chemotherapeutic temozolomide (TMZ), which is used routinely in the clinic for the treatment of glioblastoma multiforme (26), was tested in combinatorial treatment with Ad5-HRG. The estimated IC50 for TMZ was 9.58 mg/ml in the GL261 model (Figure S3). Next, glioma-bearing mice were treated with Ad5-Empty or Ad5-HRG at day 7 and 13 in combination with a suboptimal IC20 dose of TMZ. TMZ was delivered in 2 cycles, 1 mg/kg/day days 10-12 and days 16-18 (Figure S4A). This schedule was chosen to avoid, as much as possible, the induction of cytotoxicity in Ad5 transfected cells within the 48-hour period after Ad5 injection.

Consistent with previous results, Ad5-HRG treatment significantly attenuated tumor growth compared to Ad5-Empty treated tumors (Figure S4B). TMZ treatment in Ad5-Empty treated animals demonstrated no significant suppression of tumor growth, as expected given the suboptimal dose. However, TMZ treatment negated the beneficial effect of Ad5-HRG treatment.

Thus, the combination of Ad5-HRG and TMZ resulted in the same extent of tumor growth as for Ad5-Empty treated animals co-treated with DMSO/PBS vehicle (Figure S4B). Ad5-HRG treatment alone consistently resulted in a significant increase in both $CD45^+$ cell infiltration (Figure S4C) and $CD8a^+$ T cells (Figure S4D). The increase in both these cell populations in the tumor, essential for HRG's suppressive effect on tumor growth, was lost when combining Ad5-HRG with TMZ treatment. These data further support an essential role for $CD45^+$ cells in HRGs mechanism of action.

Identification of HRG-STC2 complex formation

The mechanism underlying the highly reproducible effect of HRG on the immune-modulatory profile of inflammatory cells remains poorly understood. To identify HRG's potential interaction partners on inflammatory cells, we employed the novel protein-interaction decoding technology, TRICEPS-based Ligand Receptor Capture (LRC) technology (15, 16). The TRICEPS crosslinker is equipped with three orthogonal functionalities; one arm for conjugation of the orphan ligand, in this case, HRG, a second arm for capturing oxidized carbohydrates on the putative receptor/secreted protein on living cells, and a third arm carrying a biotin tag for purification of captured receptors for subsequent analysis by quantitative mass spectrometry (MS) (Figure 4A). We applied TRICEPS-based LRC to the monocytic cell line, U937, whose differentiation to $CD14^+$ macrophages is induced by Vitamin D_3 ($VitD_3$) (29). TRICEPS-LRC identified a single interaction candidate for HRG on the cell surface of U937 cells, namely STC2 (Figure 4B; see Table 1 for MS-identification of all identified HRG-captured proteins). Additionally, we identified HRG in the HRG-capture reaction. As expected, the insulin receptor was enriched in the insulin-captured control reaction but not in the HRG-capture.

To validate the identified interaction between HRG and STC2, we used HEK293T cells endogenously expressing STC2, either lacking murine HRG expression (293WT) or overexpressing murine HRG (293HRG). The presence of HRG-STC2 complexes was examined by co-immunoprecipitation in cell culture lysate and medium. In addition, 6 hours prior to harvest, the cell culture medium was supplemented with recombinant STC2, or not, to enrich for the interaction. Anti-HRG immunoblotting of anti-STC2 immunoprecipitates demonstrated the presence of HRG in complex with STC2 in the medium from 293 HRG cultures. The HRG-STC2 interaction was enhanced by the addition of recombinant STC2 to the cell culture medium (Figure 4C). Cell lysates treated in an identical manner demonstrated a similar, but non-significant, increase in HRG in STC2 immunoprecipitates. As HEK293 cells do not express HRG endogenously (9), these data suggest that the HRG-STC2 complex is established on the cell surface and then released into the medium.

STC2 is present in gliomas in association with $CD45^+$ cells

To understand the relevance of STC2 expression in the glioma models we immunostained tissue for the presence of murine STC2 in addition to $CD45^+$ cells. STC2-positivity could be seen diffusely associated with glioma cells (Figure 5A), consistent with its secreted nature, while more intense staining was associated with $CD45^+$ cells (Figure 5B). In anti-CSF1 antibody-treated

gliomas, loss of $CD45^+$ cells (see Figure 3C) was accompanied by a loss in STC2 expression in the tumor (Figure 5A; Quantification).

To examine the consequence of the HRG-STC2 interaction on leukocytes, we utilized the U937 cell differentiation assay, on which also TRICEPS-based LRC was performed (see Figure 4B). In this assay, U937 cells differentiate towards the monocyte/macrophage lineage as assessed by CD14 expression. In agreement with previous findings (13), the addition of HRG further potentiated $VitD_3$-induced differentiation (Figure S5) in a manner dependent on the $VitD_3$ dose. When differentiated at low concentrations of $VitD_3$ (5 nM), STC2 dose-dependently suppressed CD14 expression (Figure 5C) as assessed by the number of $CD14^+$ cells and the mean fluorescence intensity of positive cells. Importantly, when included with STC2 during cell differentiation, HRG completely negated the suppressive effect of STC2. These data demonstrate that the HRG-STC2 interaction is of functional consequence in modulating leukocyte gene expression.

Microarray transcript analysis on U937 cells exposed to the different treatments showed overlapping and distinct sets of regulated genes in the four conditions: 1) VitD3 alone to induce monocytic differentiation of U937 cells, 2) combined with HRG, 3) combined with STC2 or 4) combined with HRG+STC2, compared to undifferentiated control cells. The number of regulated genes in the treatment groups was 1) VitD3 group: 538, 2) VitD3+HRG: 538, 3) VitD3+STC2: 585 and 4) VitD3+ HRG/STC2: 471 (Figure S6). Gene ontology (GO) analysis using Toppgene focused on GO categories differently regulated in the treatment groups (Supplementary Table S1). Further GO analysis was performed on the uniquely regulated genes in treatment groups 2-4 relative to VitD3 alone (Supplementary Tables S2A and S2B).

The differentially expressed VitD3+HRG genes relative VitD3 alone (group 2 vs 1) had a limited number of GO annotations (Supplementary Tables S2A, showing loss of function GO:s and S2B, showing gain of function GO:s). The differentially expressed VitD3+STC2 genes (group 3 vs 1) had the largest number of GO annotations, indicating a broader repertoire of gene regulation by STC2 than HRG on inflammatory cells. Many of the STC2-regulated genes were related to inflammation, innate immune response or acquired immune responses (51%). Surprisingly, both loss and gain of expressed genes in the VitD3+STC2 samples relative VitD3 (groups 3 vs 1) had a strong immune component (Supplementary Tables S2A-B). Importantly, inclusion of HRG in the VitD3+STC2 treatment (group 4) reduced the number of GO annotations compared to that in group 3, but the remaining gene regulation was still strongly enriched for processes related to inflammation or the immune systems (59%). Table 2 provides a summary of GO biological function described in detail in Supplementary Tables S1-2.

In conclusion, STC2 appeared to have a more dramatic effect than HRG on gene expression in U937 cells after VitD3 differentiation; treatment with STC2 in the presence of HRG eliminated certain of these gene expression changes. Many of these gene regulatory events, both quantitative and qualitative, related to the immune system.

Gene regulation in HRG-treated gliomas results in reduction in Tregs

To validate the relevance of the HRG/STC2 regulated genes described above for tumor immune responsiveness, real-time qPCR was performed on GL261 tumors harvested after treatment with buffer, Ad5-Empty or Ad5-HRG (Figure 6A). Ad5-Empty treatment induced the expression of

CD11b, CXCR4, IL-6 and interferon-γ (IFNγ). Ad5-HRG decreased gene expression of the M1 markers IL-6 and interferon (IFN)-γ whereas M2 markers were not statistically different (relative expression of Ad5-HRG treated tumor arginase-1 mRNA was 1.25 ± 0.28 and MRC1 1.78 ± 0.44 compared with buffer only treated tumors, respectively), suggesting that there is no M1 skewing of the immune system in this scenario. CD11b is a marker for myeloid cells (32), suggesting recruitment of macrophages to the tumor as a consequence of virus administration. CXCR4 is a receptor for CXCL-12 involved in immune cell retention in numerous settings (33). IL-6 and IFN-γ are pro-inflammatory cytokines, suggesting that Ad5 primed an immune response from CXCR4 positive cells and/or myeloid cells. Treatment with Ad5-HRG suppressed the gene regulatory effects to the levels seen in buffer-treated glioma and therefore, these cytokines are likely not directly involved in HRG's tumor suppressive effects but rather reflect a suppression of a general immune response against adenoviruses.

In the absence of data supporting an M1 skewing of the innate immune response, we postulated that HRG-effects on CD45/CD8 infiltration and myeloid cell differentiation in the GL261 glioma counteracted tumor-induced immune suppression. Absence of effects of HRG on gene expression of the immune checkpoint inhibitors PDL-1, PD-1 and CTLA-4 relative tumors exposed to buffer treatment only (relative expression of Ad5-HRG-treated tumors relative buffer only-treated tumors was 0.7 ± 0.5 for PDL-1, 1.2 ± 0.8 for PD-1 and 0.9 ± 0.4 for CTLA-4) targeted our focus to T regulatory cells (Tregs) as possible mediators. Tregs are known to provide an immune-suppressive tumor environment, promoting tumor growth (34, 35). We first noted that cells could be detected in the tumors that co-expressed the two IL-35 components Ebi-3 and IL-12a (Fig 6B). These were too infrequent to allow quantification by immunofluorescence staining of sections and instead FACS analysis was employed for accurate assessment of their presence. Fig 6C describes the gating strategy after staining dispersed GL261 gliomas for CD4, FoxP3, Ebi3 and IL-12a. As shown in Fig 6D, HRG-treated gliomas exhibited fewer IL-35 expressing Tregs, providing an explanation for the increased infiltration of CD45/CD8+ cells and reduced tumor growth.

Discussion

The mechanistic understanding of HRG's anti-tumor effects, underlying the exploration of its usefulness as a cancer therapeutic, derives from studies on peripheral, non-CNS tumor models in mice. The effect of HRG in tumor growth and spread has been studied by delivering purified recombinant protein, HRG-derived peptides, or by expressing HRG in tumor cells (9, 11, 13, 36). One study demonstrated that HRG expression in an orthotopic murine glioma model (RCAS/TV-A) resulted in a reduction in tumor incidence and, strikingly, the absence of grade 4 lesions, as assessed by mitotic index and vessel density (37). This indicated that HRG may be therapeutically beneficial also for tumors in the CNS. Herein, we have developed an adenovirus-based vector encoding HRG to allow for local delivery of HRG to the tumor site thereby circumventing the need for systemic delivery. HRG-gene therapy demonstrated significant and robust inhibition of tumor growth. HRG-treated gliomas displayed an increased number of perfused vessels, in line with previous observations of the ability of HRG to normalize the tumor

vasculature (11). $CD45^+$ and T cell numbers were increased in HRG-treated tumors compared to controls. The immune regulatory cytokine profile in HRG-treated gliomas showed that HRG suppressed immune modulatory effects seen in gliomas treated with the Ad5 virus alone. Changes in Ad5-Empty treated gliomas were compatible with inflammatory cell recruitment. In contrast, Ad5-HRG administration reduced expression of Tregs expressing the immune-suppressive dimeric cytokine IL-35, composed of IL-12a and Ebi3/IL-27β (38). Tregs expressing this cytokine have in many instances been shown to promote tumor expansion (34, 35). The related cytokine IL-12, composed of IL-12α and IL-12β on the other hand, is a potent inducer of anti-tumor immunity (39). It was recently shown that oncolytic virus-delivery of IL-12 to murine glioma results in enhanced T effector-mediated anti-tumor response and suppressed Treg infiltration (40). Moreover, the combination of oncolytic IL-12 delivery with neutralization of checkpoint inhibitors PD1 and CTLA-4 dramatically blocks murine glioma growth (41). The strong preclinical effects of checkpoint inhibitors have promoted clinical trials for treatment of glioblastoma multiforme either as monotherapy or in a wide range of combinatorial treatments (42). Treg suppressive treatment, in the longer perspective potentially based on a HRG mimetic, may have a very good potential to be efficacious in such combinatorial glioma therapy.

Ad5-HRGs mechanism of action in gliomas replicated that reported previously for peripheral tumors as depletion of $CSFR1^+$ cells negated the beneficial effect of HRG (3, 11). The use of the chemotherapeutic TMZ in combination with HRG also antagonized the effects of HRG, likely through a similar mechanism, i.e. the depletion of $CSFR1^+$ cells. Indeed, a number of murine studies have demonstrated the significant depletion of monocytes, and consequently macrophages, following TMZ treatment, even at sub-therapeutic concentration (43). While this study highlights the potential utility of HRG for glioma treatment, it also identifies potential challenges when combined with monocyte/macrophage cell targeting therapeutics, particularly of note since TMZ is the frontline grade 4 glioma chemotherapeutic.

Despite the robust effects of HRG on tumors both peripherally and in the CNS there still remains a lack of understanding of exactly how HRG exerts its effects on inflammatory cells. To address this important question, we used the recently developed protein interaction decoding technology, TRICEPS-based LRC (15, 16, 18), to identify HRG interaction partners on the cell surface of an inflammatory cell model. TRICEPS is a tri-valent linker molecule simultaneously binding the orphan ligand, the N-glycosylated putative receptor/interaction partner at the cell surface, as well as streptavidin for purification. HRG-coupled TRICEPS followed by mass spectrometry identified STC2 as previously unknown interaction partner candidate of HRG in differentiated U937 cells.

The interaction between HRG and STC2 was further validated by co-immunoprecipitation. In $VitD_3$-treated U937 cells, STC2 negatively regulated $CD14^+$ cell differentiation, in line with the described ability of peptides derived from STC1 and STC2 to directly affect inflammatory cell function (44). Crucially, transcript analyses in U937 cells treated with HRG or STC2 individually or in combination indicated that HRG modulated certain immunoregulatory changes seen in STC2-treated cells. Whether the HRG/STC2 complex neutralizes STC2 directly or if HRG modulates STC2's biology for example by regulation of a potential STC2 receptor on inflammatory cells, is unknown at this point. It is noteworthy that while HRG can be retained by binding to cell surface-expressed heparan sulfate (4), specific, saturable binding of HRG occurs to inflammatory cells, independently of heparan sulfate (3).

Taken together our data suggest that STC2 and HRG can directly interact and modulate the phenotype of inflammatory cells. Another possible mechanism of action for the HRG-STC2 complex may involve the reported cytoprotective effects of STC2 (45). Thus, HRG might sensitize tumor cells to ER stress by neutralizing STC2. HRG may also synergize with other small molecule effectors of ER stress e.g. small-molecule plant compounds that bind to GRP78 (46). An interesting compound in this regard is Honokiol, which confers immunogenicity by regulating calreticulin exposure, activating ER stress and inhibiting epithelial-to-mesenchymal transition (47).

In vivo, the significance of the HRG/STC2 interaction remains to be explored fully. The observation that both tumor cells and $CD45^+$ cells expressed STC2 in the glioma model shows 1) that STC2 is present in the tumor microenvironment where HRG is known to act and moreover, 2) that STC2 is expressed by inflammatory cells, which HRG has been shown to directly influence. Thus, HRG may steer tumor development by direct interaction with STC2 on or proximal to inflammatory cells, modulating their phenotype.

Here, we have demonstrated the applicability of HRG therapy in an adenovirus gene-therapy based system, showing that local HRG delivery to the tumor site is a feasible approach. We have successfully applied this to an *in vivo* glioma model and demonstrated that the mechanism of action is in part distinct relative HRG's effects in peripheral tumor models. While HRG promotes efficient tumor vessel perfusion and infiltration of CD8+ cells in both situations, the M1/M2 polarization noted in peripheral tumors (11) is not established in gliomas. Instead, in gliomas, HRG acts to balance the immunomodulatory effects of STC2, correlating with a reduction in Treg infiltration. It remains to be assessed as to whether HRG therapy, in gliomas, acts through both microglia and infiltrating macrophages and if gene-expression changes in these two distinct populations differentially contribute to HRGs effects. This study also highlights the potential antagonism between HRG and therapies that target macrophage/myeloid cell populations while simultaneously potentially promoting immune checkpoint therapy.

Cancer is a leading cause of death in the industrialized world and to an increasing extent a cause of death in developing countries. While our understanding of common features of signaling and metabolic aberrations in cancer is increasing, it is clear that cancer is highly heterogenous and adapts in response to therapies. Novel therapies, possibly administered in a sequential manner and acting to induce tissue homeostasis are therefore urgently needed (48). HRG-gene therapy in the CNS offers novel and distinct advantages above current therapeutics. The ability to normalize the glioma vasculature has the potential to enhance therapeutic delivery similar to the effect of the anti-VEGF antibody Bevacizumab. Additionally, the suppression of immunosuppressive TAMs or Tregs in the tumor may enhance anti-tumor immune response, which may be particularly relevant in combination with immunostimulatory antibody therapeutics. Finally, the identification of STC2 as a partner for HRG in regulation of $CD45^+$ cell phenotype presents a new concept where serum proteins appearing in different constellations serve as endogenous rheostats to steer the tumor inflammation profile in pro- or anti-tumor directions.

Acknowledgements

We thank Marie Hedlund, Uppsala University for expert technical assistance with the glioma model. We also thank Pernilla Martinsson, Uppsala University for expert technical assistance on biochemical analyses and Berith Nilsson, Uppsala University, for expert technical assistance in the production of recombinant adenoviruses. We also acknowledge the contribution of the Array and Analysis Facility, Uppsala University. In particular, expert evaluation by Drs. Pascal Pucholt, Dept. Medical Sciences and Dr. Lei Lui Conze, Dept. Immunology, Genetics and Pathology, is greatly appreciated.

Funding

This study was supported by grants from the Swedish Cancer Society (16 0585), the Swedish Research Council (2015-02375_3) and a Wallenberg Scholar grant from the Knut and Alice Wallenberg foundation to L.C.W., and from the Swedish Cancer Society (16 0520), and the Swedish Research Council (2016-01085) to M.W.

Authorship

Contribution: F.P.R., I.P., E.O.S., M.E., M.W. and L.C.W. conceived and designed the study and wrote the primary and subsequent versions of the manuscript; F.P.R., E.O.S., O.N., H.K., B.W., I.P. and N.S. conducted and/or designed laboratory experiments; M.W: conducted bioinformatics analyses; all coauthors reviewed and edited the manuscript.

Correspondence: Lena Claesson-Welsh, Uppsala University, Department of Immunology, Genetics and Pathology, The Rudbeck Laboratory, Dag Hammarskjöldv. 20, 751 85 Uppsala, Sweden. E-mail lena.welsh@igp.uu.se, or phone +46-70 167 9260.

References

1. Poon IK, Patel KK, Davis DS, Parish CR, Hulett MD. Histidine-rich glycoprotein: the Swiss Army knife of mammalian plasma. Blood. 2011;117:2093-101.
2. Koide T, Foster D, Yoshitake S, Davie EW. Amino acid sequence of human histidine-rich glycoprotein derived from the nucleotide sequence of its cDNA. Biochemistry. 1986;25:2220-5.
3. Tugues S, Roche F, Noguer O, Orlova A, Bhoi S, Padhan N, et al. Histidine-rich glycoprotein uptake and turnover is mediated by mononuclear phagocytes. PLoS One. 2014;9:e107483.
4. Vanwildemeersch M, Olsson AK, Gottfridsson E, Claesson-Welsh L, Lindahl U, Spillmann D. The anti-angiogenic His/Pro-rich fragment of histidine-rich glycoprotein binds to endothelial cell heparan sulfate in a Zn2+-dependent manner. J Biol Chem. 2006;281:10298-304.
5. Manderson GA, Martin M, Onnerfjord P, Saxne T, Schmidtchen A, Mollnes TE, et al. Interactions of histidine-rich glycoprotein with immunoglobulins and proteins of the complement system. Mol Immunol. 2009;46:3388-98.
6. Gorgani NN, Theofilopoulos AN. Contribution of histidine-rich glycoprotein in clearance of immune complexes and apoptotic cells: implications for ameliorating autoimmune diseases. Autoimmunity. 2007;40:260-6.
7. Priebatsch KM, Kvansakul M, Poon IK, Hulett MD. Functional Regulation of the Plasma Protein Histidine-Rich Glycoprotein by Zn2+ in Settings of Tissue Injury. Biomolecules. 2017;7.
8. Shannon O, Rydengard V, Schmidtchen A, Morgelin M, Alm P, Sorensen OE, et al. Histidine-rich glycoprotein promotes bacterial entrapment in clots and decreases mortality in a mouse model of sepsis. Blood. 2010;116:2365-72.
9. Olsson AK, Larsson H, Dixelius J, Johansson I, Lee C, Oellig C, et al. A fragment of histidine-rich glycoprotein is a potent inhibitor of tumor vascularization. Cancer Res. 2004;64:599-605.
10. Roche F, Sipila K, Honjo S, Johansson S, Tugues S, Heino J, et al. Histidine-rich glycoprotein blocks collagen-binding integrins and adhesion of endothelial cells through low-affinity interaction with alpha2 integrin. Matrix biology : journal of the International Society for Matrix Biology. 2015;48:89-99.
11. Rolny C, Mazzone M, Tugues S, Laoui D, Johansson I, Coulon C, et al. HRG inhibits tumor growth and metastasis by inducing macrophage polarization and vessel normalization through downregulation of PlGF. Cancer Cell. 2011;19:31-44.
12. Sica A, Erreni M, Allavena P, Porta C. Macrophage polarization in pathology. Cell Mol Life Sci. 2015;72:4111-26.
13. Tugues S, Honjo S, Konig C, Noguer O, Hedlund M, Botling J, et al. Genetic deficiency in plasma protein HRG enhances tumor growth and metastasis by exacerbating immune escape and vessel abnormalization. Cancer Res. 2012;72:1953-63.
14. Tsuchida-Straeten N, Ensslen S, Schafer C, Woltje M, Denecke B, Moser M, et al. Enhanced blood coagulation and fibrinolysis in mice lacking histidine-rich glycoprotein (HRG). J Thromb Haemost. 2005;3:865-72.
15. Frei AP, Jeon OY, Kilcher S, Moest H, Henning LM, Jost C, et al. Direct identification of ligand-receptor interactions on living cells and tissues. Nat Biotechnol. 2012;30:997-1001.
16. Frei AP, Moest H, Novy K, Wollscheid B. Ligand-based receptor identification on living cells and tissues using TRICEPS. Nat Protoc. 2013;8:1321-36.
17. Chang AC, Hook J, Lemckert FA, McDonald MM, Nguyen MA, Hardeman EC, et al. The murine stanniocalcin 2 gene is a negative regulator of postnatal growth. Endocrinology. 2008;149:2403-10.

18. Bouras T, Southey MC, Chang AC, Reddel RR, Willhite D, Glynne R, et al. Stanniocalcin 2 is an estrogen-responsive gene coexpressed with the estrogen receptor in human breast cancer. Cancer Res. 2002;62:1289-95.
19. Volland S, Kugler W, Schweigerer L, Wilting J, Becker J. Stanniocalcin 2 promotes invasion and is associated with metastatic stages in neuroblastoma. Int J Cancer. 2009;125:2049-57.
20. Proserpio V, Piccolo A, Haim-Vilmovsky L, Kar G, Lonnberg T, Svensson V, et al. Single-cell analysis of CD4+ T-cell differentiation reveals three major cell states and progressive acceleration of proliferation. Genome Biol. 2016;17:103.
21. Stoll G, Enot D, Mlecnik B, Galon J, Zitvogel L, Kroemer G. Immune-related gene signatures predict the outcome of neoadjuvant chemotherapy. Oncoimmunology. 2014;3:e27884.
22. Delgado-Lopez PD, Corrales-Garcia EM. Survival in glioblastoma: a review on the impact of treatment modalities. Clin Transl Oncol. 2016;18:1062-71.
23. Field KM, Jordan JT, Wen PY, Rosenthal MA, Reardon DA. Bevacizumab and glioblastoma: scientific review, newly reported updates, and ongoing controversies. Cancer. 2015;121:997-1007.
24. Corbett TH, Roberts BJ, Leopold WR, Peckham JC, Wilkoff LJ, Griswold DP, Jr., et al. Induction and chemotherapeutic response of two transplantable ductal adenocarcinomas of the pancreas in C57BL/6 mice. Cancer Res. 1984;44:717-26.
25. He TC, Zhou S, da Costa LT, Yu J, Kinzler KW, Vogelstein B. A simplified system for generating recombinant adenoviruses. Proc Natl Acad Sci U S A. 1998;95:2509-14.
26. Golde WT, Gollobin P, Rodriguez LL. A rapid, simple, and humane method for submandibular bleeding of mice using a lancet. Lab Anim (NY). 2005;34:39-43.
27. Szatmari T, Lumniczky K, Desaknai S, Trajcevski S, Hidvegi EJ, Hamada H, et al. Detailed characterization of the mouse glioma 261 tumor model for experimental glioblastoma therapy. Cancer Sci. 2006;97:546-53.
28. Lal S, Lacroix M, Tofilon P, Fuller GN, Sawaya R, Lang FF. An implantable guide-screw system for brain tumor studies in small animals. J Neurosurg. 2000;92:326-33.
29. Dodd RC, Cohen MS, Newman SL, Gray TK. Vitamin D metabolites change the phenotype of monoblastic U937 cells. Proc Natl Acad Sci U S A. 1983;80:7538-41.
30. MacDonald KP, Palmer JS, Cronau S, Seppanen E, Olver S, Raffelt NC, et al. An antibody against the colony-stimulating factor 1 receptor depletes the resident subset of monocytes and tissue- and tumor-associated macrophages but does not inhibit inflammation. Blood. 2010;116:3955-63.
31. Zhu Y, Knolhoff BL, Meyer MA, Nywening TM, West BL, Luo J, et al. CSF1/CSF1R blockade reprograms tumor-infiltrating macrophages and improves response to T-cell checkpoint immunotherapy in pancreatic cancer models. Cancer Res. 2014;74:5057-69.
32. Kong YY, Fuchsberger M, Xiang SD, Apostolopoulos V, Plebanski M. Myeloid derived suppressor cells and their role in diseases. Curr Med Chem. 2013;20:1437-44.
33. Guo F, Wang Y, Liu J, Mok SC, Xue F, Zhang W. CXCL12/CXCR4: a symbiotic bridge linking cancer cells and their stromal neighbors in oncogenic communication networks. Oncogene. 2016;35:816-26.
34. Chen G, Liang Y, Guan X, Chen H, Liu Q, Lin B, et al. Circulating low IL-23: IL-35 cytokine ratio promotes progression associated with poor prognosisin breast cancer. Am J Transl Res. 2016;8:2255-64.
35. Chang AL, Miska J, Wainwright DA, Dey M, Rivetta CV, Yu D, et al. CCL2 Produced by the Glioma Microenvironment Is Essential for the Recruitment of Regulatory T Cells and Myeloid-Derived Suppressor Cells. Cancer Res. 2016;76:5671-82.

36. Juarez JC, Guan X, Shipulina NV, Plunkett ML, Parry GC, Shaw DE, et al. Histidine-proline-rich glycoprotein has potent antiangiogenic activity mediated through the histidine-proline-rich domain. Cancer Res. 2002;62:5344-50.
37. Karrlander M, Lindberg N, Olofsson T, Kastemar M, Olsson AK, Uhrbom L. Histidine-rich glycoprotein can prevent development of mouse experimental glioblastoma. PLoS One. 2009;4:e8536.
38. Collison LW, Workman CJ, Kuo TT, Boyd K, Wang Y, Vignali KM, et al. The inhibitory cytokine IL-35 contributes to regulatory T-cell function. Nature. 2007;450:566-9.
39. Tugues S, Burkhard SH, Ohs I, Vrohlings M, Nussbaum K, Vom Berg J, et al. New insights into IL-12-mediated tumor suppression. Cell Death Differ. 2015;22:237-46.
40. Cheema TA, Wakimoto H, Fecci PE, Ning J, Kuroda T, Jeyaretna DS, et al. Multifaceted oncolytic virus therapy for glioblastoma in an immunocompetent cancer stem cell model. Proc Natl Acad Sci U S A. 2013;110:12006-11.
41. Saha D, Martuza RL, Rabkin SD. Macrophage Polarization Contributes to Glioblastoma Eradication by Combination Immunovirotherapy and Immune Checkpoint Blockade. Cancer Cell. 2017;32:253-67 e5.
42. Maxwell R, Jackson CM, Lim M. Clinical Trials Investigating Immune Checkpoint Blockade in Glioblastoma. Curr Treat Options Oncol. 2017;18:51.
43. Briegert M, Kaina B. Human monocytes, but not dendritic cells derived from them, are defective in base excision repair and hypersensitive to methylating agents. Cancer Res. 2007;67:26-31.
44. Yamamoto K, Tajima Y, Hasegawa A, Takahashi Y, Kojima M, Watanabe R, et al. Contrasting effects of stanniocalcin-related polypeptides on macrophage foam cell formation and vascular smooth muscle cell migration. Peptides. 2016;82:120-7.
45. Ito D, Walker JR, Thompson CS, Moroz I, Lin W, Veselits ML, et al. Characterization of stanniocalcin 2, a novel target of the mammalian unfolded protein response with cytoprotective properties. Mol Cell Biol. 2004;24:9456-69.
46. Martin S, Lamb HK, Brady C, Lefkove B, Bonner MY, Thompson P, et al. Inducing apoptosis of cancer cells using small-molecule plant compounds that bind to GRP78. Br J Cancer. 2013;109:433-43.
47. Liu SH, Lee WJ, Lai DW, Wu SM, Liu CY, Tien HR, et al. Honokiol confers immunogenicity by dictating calreticulin exposure, activating ER stress and inhibiting epithelial-to-mesenchymal transition. Mol Oncol. 2015;9:834-49.
48. Arbiser JL, Bonner MY, Gilbert LC. Targeting the duality of cancer. NPJ Precis Oncol. 2017;1.

Table 1. List of HRG-TRICEPS captured proteins identified by mass spectrometry

Candidate (Uniprot)	Fold-change	Adj p-value (protein level)
Stanniocalcin-2, STC2 (O76061)	91.72	0.00920075
Protein kinase C-binding protein, NELL2 (Q99435)	167.57	0.263903936
Calsyntein-1, CLSN1 (O94985)	27.52	0.527681447
IL-17 receptor A, IL17RA (Q96F46)	14.04	0.39207134
Butyrophilin subfamily 2 member A1, BTN2A1 (Q7KYR7)	10.60	0.178244686
Lysosome-associated membrane glycoprotein 1, LAMP1 (P11279)	8.38	0.527681447
Protein HEG homolog 1, HEG1 (Q9UL13)	2.19	0.086966529

Table 2. Biological processes induced by HRG, STC2 or the combination

Summary of changes in biological processes related to inflammatory/immune functions relative vitamin D3 alone as presented in detail in Supplementary Tables 1 and 2.

HRG + VitD3	STC2 + VitD3	HRG + STC2 + VitD3
• TLR 5 signaling	• TLR 5 signaling • Cytokine production/function • Lymphocyte proliferation • Mononuclear cell proliferation • Leukocyte migration • Regulation of immune system • Regulation of NF-kappaB • Immune response • Lymphocyte activation • Lymphocyte migration • Activation of innate immunity • TIRAP-dependent TLR • Chemokine production • Granzyme B production	• TLR 5 signaling • Immune response • Immune system process • Inflammatory response • Neutrophil chemotaxis • Cytokine production/function • Lymphocyte activation • Immune system development • T cell differentiation • TIRAP-dependent TLR • Innate immune response

Abbreviations: TLR; toll-like receptor, TIRAP; toll-interleukin 1 receptor domain containing adaptor protein, NFkappaB; nuclear factor of kappa light polypeptide gene enhancer in B-cells

Figures legends

Figure 1. Adenovirus vector-mediated HRG expression *in vivo*

(A) *In* vivo expression by Ad5 adenovirus vectors. Subcutaneous Panc02 tumors were established in mice and injected with $1x10^8$ ffu of Ad5-HRG-Luc and luciferase activity assessed by *in vivo* luciferase imaging (n=5). (B) *In vivo* expression of HRG by Ad5 vectors: Subcutaneous Panc02 tumors were established in mice and injected with $1x10^8$ ffu of Ad5-HRG, Ad5-Empty vectors or buffer. HRG expression was quantified from tumor lysates by ELISA 48 hours later (n=3). (C) Growth of subcutaneous Panc02 tumors treated with adenovirus vectors (n=10-11 per treatment). Tumors were injected with $1x10^8$ ffu of Ad5-HRG, Ad5-Empty or Buffer. Once reaching an average tumor volume of 50 mm^3 (Day 0) tumors were treated every 4 days for 4 treatments (indicated by arrowheads). (D) Final tumor weight of subcutaneous Panc02 tumors from C. Error bars represent SEM. Statistical analyses were performed using one-way ANOVA followed by Fisher's LSD test (B) or Tukey's post hoc test. *, $p<0.05$, **, $p<0.01$.

Figure 2. Ad5-HRG treatment of intracranial glioma

(A) Schematic of treatment strategy. Screws were implanted into the skull and one week later (day 1) 7,500 GL261 cells were inoculated into the caudate nucleus. Ad5 vectors were delivered at day 7 and 13 and the experiment ended 21 days after GL261 cell inoculation. (B) GL261 tumor volumes at the experimental endpoint (expressed as a percentage of buffer-treated tumors, left). Scale bar represents 100 µm. Representative H&E staining of *in situ* tumors (right). (C) Quantification of number of perfused vessels in GL261 tumors (left). Representative IF images of perfused vessels in tumors (right): blue; 4,6 diamidino-2-phenylindole(DAPI)/nuclei, green; biotinylated lectin/perfused vessels, red; automatic outlining of vessels. (D) Quantification of $CD45^+$ cells in GL261 tumors (left). Representative IF images of tumors (right); blue; DAPI/nuclei, green; CD45. GL261 treatment experiments were performed using 8-12 mice per group, and carried out in 3 independent replicates using two independently produced and titered batches of AdV5 vectors. Error bars represent SEM. Scale bar; 100 µm. Statistical analyses were done using one-way ANOVA followed by Tukey's post hoc test (C) or one-way ANOVA followed by Bonferroni post hoc and Students' t-test (B). Chi square test was used in D to compare Ad5 alone with Ad5-HRG when using median value (3.2) as cut-off between positive and negative values. *, $p<0.05$, **, $p<0.01$.

Figure 3. Neutralization of CSF1 and Ad5-HRG treatment

(A) Schematic of treatment strategy. Screws were implanted into the skull and one week later (day 1) 7,500 GL261 cells were inoculated into the caudate nucleus (n=8-12 mice per group). Ad5 vectors were delivered at day 7 and 13 and the experiment ended 21 days after GL261 cell inoculation. Neutralizing αCSF1 antibody was delivered by intraperitoneal injection at day 2 (1 mg/mouse) and days 6, 10 and 14 (0.5 mg/mouse). (B) GL261 tumor sizes at the experimental endpoint expressed as a percentage of buffer-treated tumors with each experimental arm. (C)

Quantification of $CD45^+$ cells. (D) Quantification of $CD8a^+$ cells. Error bars represent SEM. Statistical analyses were done using one-way ANOVA followed by Tukey's post hoc test (C,D) or one-way ANOVA followed by Bonferroni post hoc and Students' t-test (B). *, $p<0.05$. ns; not significant.

Figure 4. Identification of STC2 as an HRG interaction partner

(A) Schematic of TRICEPS compound. Red; biotin-coupled group for streptavidin-binding, green; amine-reactive group for binding of the bait (insulin, HRG), blue; aldehyde-reactive group for binding to oxidized carbohydrates. (B) Results of TRICEPS-based LRC with HRG (sample ligand) and insulin (control ligand) on U937 cells. Candidate receptors are defined as having an FDR (false discovery rate)-adjusted p-value of 0.01 or less and a fold change of greater than 2 for HRG-captured receptors or smaller than -2 for insulin-captured receptors. Indicated are HRG (the orphan ligand), STC2 (putative receptor) and insulin receptor (INSR, receptor identified in technical control capture with insulin). (C) Immunoprecipitation of HRG-STC2 complexes. Representative images of immunoblotting (left) for STC2 (upper panel) and HRG (lower panel) on immunoprecipitates of STC2 from untransfected HEK293 (293 WT) or transfected with mouse HRG cDNA (293 HRG). Note that HEK293 cells express STC2 endogenously, in addition, 5 μg/ml purified, recombinant STC2 was added to the medium. Quantification of 5 independent replicates (right panel). Error bars represent SEM. One-way ANOVA; *, $p<0.05$.

Figure 5. STC2 is expressed in gliomas and co-localises with $CD45^+$ cells

(A) Representative images of STC2 and CD45 co-staining in Ad5-Empty and Ad5-HRG treated mouse glioma. CD45 (red), STC2 (green) and nuclei (blue) and merged image. Scale bar represents 100 μm. Panel below shows quantification of CD45 and STC2 immunoreactivity in gliomas treated or not with anti-CSF1 neutralizing antibodies (n=3-4). Error bars represent SEM. **, $p<0.01$. (B) Representative image of co-localization of STC2 and HRG. CD45 (red), STC2 (green) and nuclei (blue) and merged image. Scale bar represents 10 μm. (C) U937 cell differentiation assay induced by 5 nM $VitD_3$. Flow cytometric quantification of $CD14^+$ cells as % positive cells (left) and mean fluorescent intensity (right). Data points are the averages for triplicate or quadruplicate samples; error bars represent SEM. Statistical analysis was done using one-way ANOVA (D). **$p<0.01$; ****$p<0.0001$.

Figure 6. Gene expression and Tregs in Ad5-HRG-treated gliomas

(A) qPCR of immuno-modulatory genes listed on the x-axis; changes relative to b-actin. Samples derived from gliomas in mice treated with buffer, Ad5-Empty or Ad5-HRG. (B) Immunostaining of glioma sections from mice treated with Ad5-HRG (upper) or Ad5-Empty (lower) for Ebi3 (green) and IL-12 (red) shown individually and merged. DAPI shows position of nuclei. One-way ANOVA followed by Tukey's or Bonferroni's post hoc test were used. *, $p<0.05$, **, $p<0.01$, ***, $p<0.001$.

(C) FACS profiles and gating strategy for IL-35^{+} Tregs. Cells were first gated for CD4/FoxP3 double positive cells. These were then gated for IL-35 (Ebi3/IL-12a double positive) expressing cells. Percentages of parent cell populations are given. (D) Quantitation of total IL-35 positive Tregs in tumors. Means ± SEM are given for n=3 buffer, n=3 for Ad5 only and n=6 Ad5-HRG. ** indicates $p< 0.01$ by Student t-test.

Figure 1. Roche

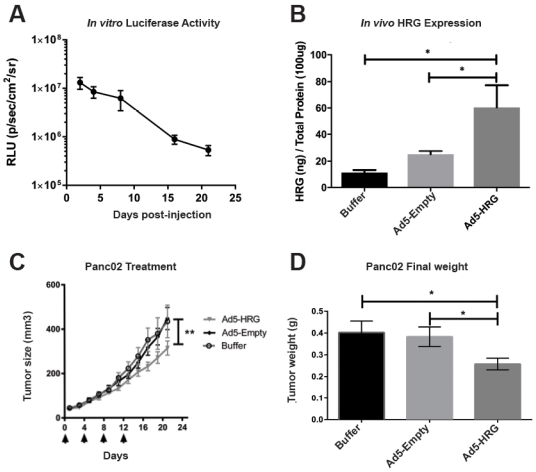

Figure 2

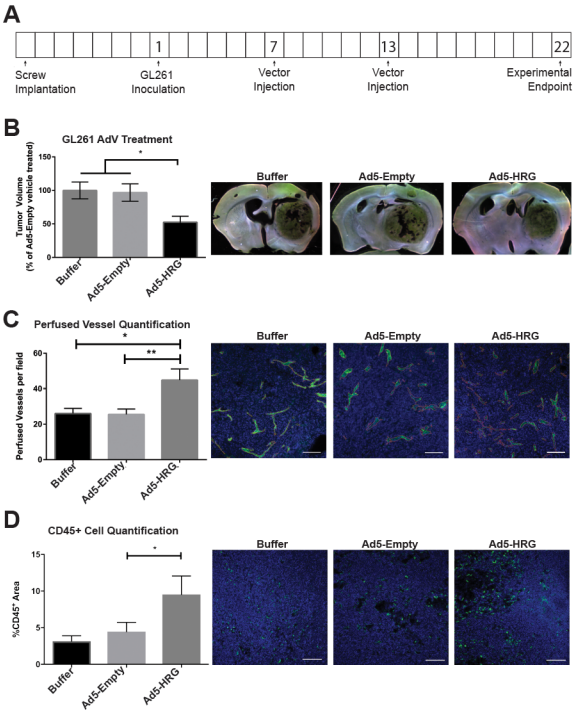
A
1
7
13
22
Screw Implantation
GL261 Inoculation
Vector Injection
Vector Injection
Experimental Endpoint
B
GL261 AdV Treatment
Tumor Volume (% of Ad5-Empty vehicle treated)
150
100
50
0
*
Buffer
Ad5-Empty
Ad5-HRG
Buffer
Ad5-Empty
Ad5-HRG
C
Perfused Vessel Quantification
Perfused Vessels per field
60
40
20
0
*
**
Buffer
Ad5-Empty
Ad5-HRG
Buffer
Ad5-Empty
Ad5-HRG
D
CD45+ Cell Quantification
%CD45+ Area
15
10
5
0
*
Buffer
Ad5-Empty
Ad5-HRG
Buffer
Ad5-Empty
Ad5-HRG

Figure 3

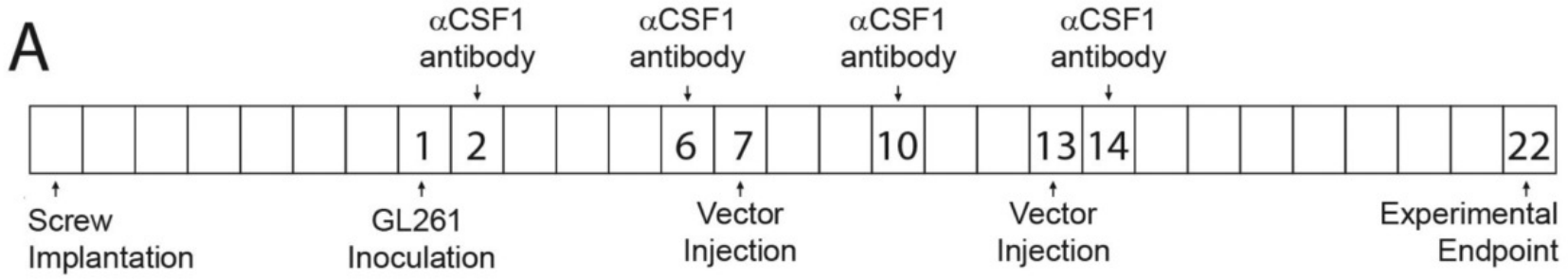
A
αCSF1 antibody
αCSF1 antibody
αCSF1 antibody
αCSF1 antibody
1
2
6
7
10
13
14
22
Screw Implantation
GL261 Inoculation
Vector Injection
Vector Injection
Experimental Endpoint

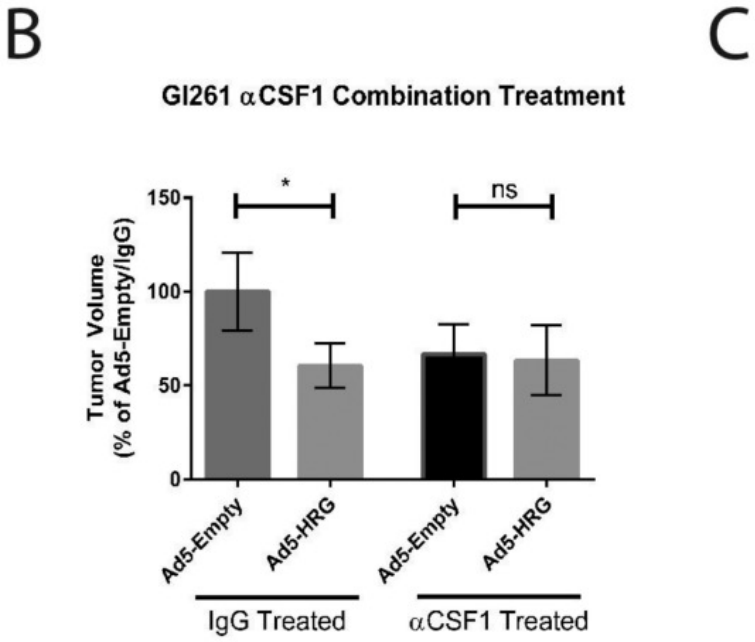
B
Gl261 αCSF1 Combination Treatment
Tumor Volume (% of Ad5-Empty/IgG)
150
100
50
0
*
ns
Ad5-Empty
Ad5-HRG
Ad5-Empty
Ad5-HRG
IgG Treated
αCSF1 Treated

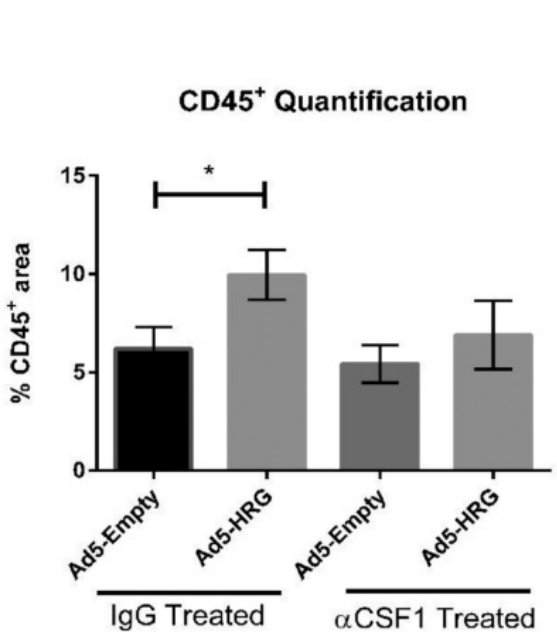
C
CD45+ Quantification
% CD45+ area
15
10
5
0
*
Ad5-Empty
Ad5-HRG
Ad5-Empty
Ad5-HRG
IgG Treated
αCSF1 Treated

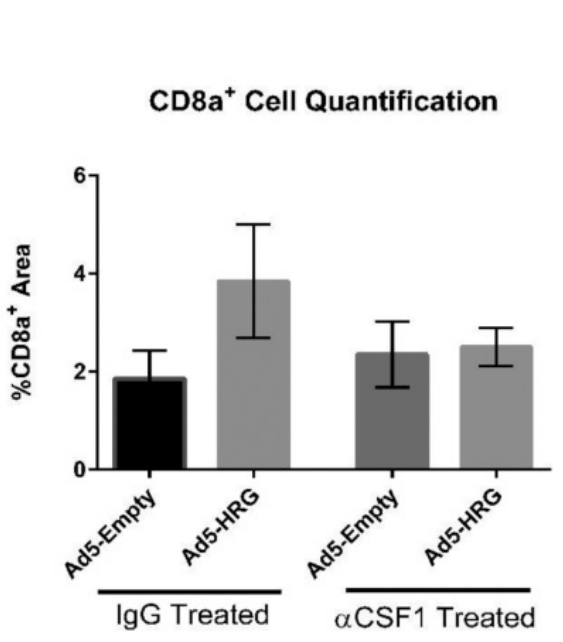
D
CD8a+ Cell Quantification
%CD8a+ Area
6
4
2
0
Ad5-Empty
Ad5-HRG
Ad5-Empty
Ad5-HRG
IgG Treated
αCSF1 Treated

Figure 4

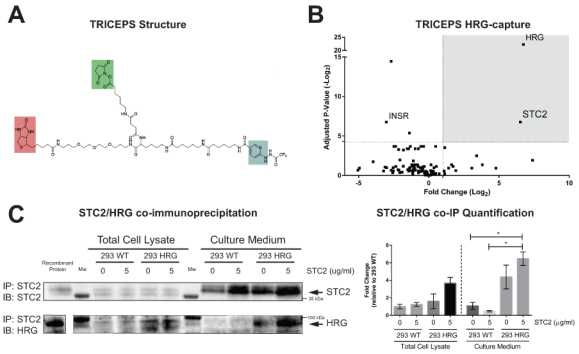
A
TRICEPS Structure
B
TRICEPS HRG-capture
HRG
INSR
STC2
Adjusted P-Value (-Log2)
Fold Change (Log2)
C
STC2/HRG co-immunoprecipitation
Total Cell Lysate
Culture Medium
293 WT
293 HRG
Recombinant Protein
Mw
STC2 (ug/ml)
IP: STC2
IB: STC2
IP: STC2
IB: HRG
STC2
HRG
STC2/HRG co-IP Quantification
Fold Change (relative to 293 WT)
STC2 (µg/ml)
Total Cell Lysate
Culture Medium

Figure 5. Roche

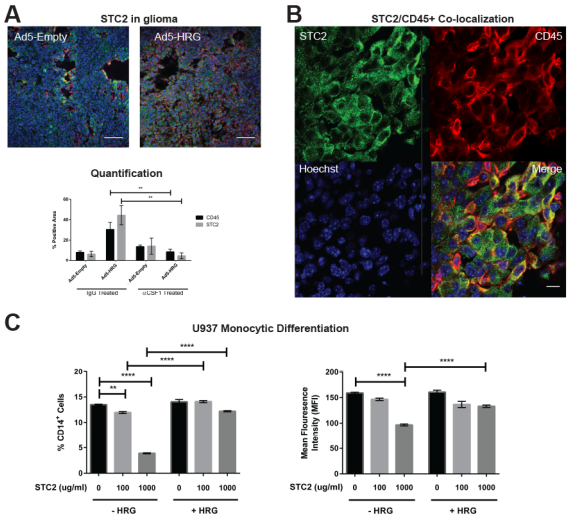

Figure 6

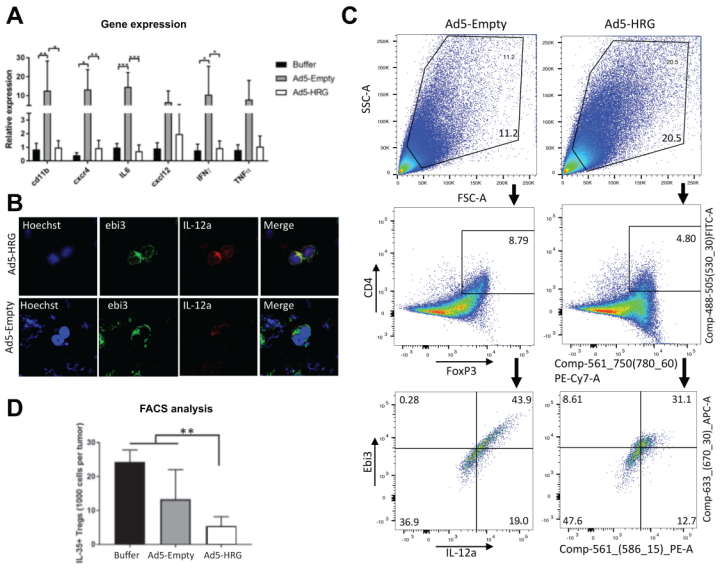
A
Gene expression
Relative expression
Buffer
Ad5-Empty
Ad5-HRG
cxcl1b
cxcr4
IL6
cxcl12
IFNγ
TNFα
B
Ad5-HRG
Ad5-Empty
Hoechst
ebi3
IL-12a
Merge
C
Ad5-Empty
Ad5-HRG
SSC-A
FSC-A
11.2
20.5
CD4
FoxP3
8.79
4.80
Comp-488-505(530_30)FITC-A
Comp-561_750(780_60)
PE-Cy7-A
Ebi3
IL-12a
0.28
43.9
36.9
19.0
8.61
31.1
47.6
12.7
Comp-633_(670_30)_APC-A
Comp-561_(586_15)_PE-A
D
FACS analysis
IL-35+ Tregs (1000 cells per tumor)
**
Buffer
Ad5-Empty
Ad5-HRG